

Full Point Encoding for Local Feature Aggregation in 3D Point Clouds

Yong He, Hongshan Yu, Zhengeng Yang, Xiaoyan Liu, Wei Sun, Ajmal Mian

Abstract—Point cloud processing methods exploit local point features and global context through aggregation which does not explicitly model the internal correlations between local and global features. To address this problem, we propose full point encoding which is applicable to convolution and transformer architectures. Specifically, we propose Full Point Convolution (FPConv) and Full Point Transformer (FPTransformer) architectures. The key idea is to adaptively learn the weights from local and global geometric connections, where the connections are established through local and global correlation functions respectively. FPConv and FPTransformer simultaneously model the local and global geometric relationships as well as their internal correlations, demonstrating strong generalization ability and high performance. FPConv is incorporated in classical hierarchical network architectures to achieve local and global shape-aware learning. In FPTransformer, we introduce full point position encoding in self-attention, that hierarchically encodes each point position in the global and local receptive field. We also propose a shape aware downsampling block which takes into account the local shape and the global context. Experimental comparison to existing methods on benchmark datasets show the efficacy of FPConv and FPTransformer for semantic segmentation, object detection, classification, and normal estimation tasks. In particular, we achieve state-of-the-art semantic segmentation results of 76% mIoU on S3DIS 6-fold and 72.2% on S3DIS Area 5.

Index Terms—Deep learning, 3D point clouds, Convolution, Transformer, Local features, Global Context

I. INTRODUCTION

Point cloud processing has drawn considerable research interest due to its wide range of applications in autonomous driving [1]–[3], robotics [4], and industrial automation [5]. Learning effective features from raw point clouds is difficult due to its irregular nature. Early methods transformed points into regular grids (e.g. multi-view images [6], [7], voxels [8], [9]), for seamless application of grid convolutions. However, the discretization process inevitably sacrifices important geometric information, distorts object shapes and results in a huge computational overhead.

To learn features from raw point clouds, the pioneering work PointNet [10] employs shared multi-layer perceptrons

Yong He, Hongshan Yu, Zhengeng Yang, Xiaoyan Liu, Wei Sun are with the National Engineering Laboratory for Robot Visual Perception and Control Technology, College of Electrical and Information Engineering, Hunan University, Lushan South Rd., Yuelu Dist., 410082, Changsha, China. This work was partially supported by the National Natural Science Foundation of China (Grants U2013203, 61973106).

Ajmal Mian is with the Department of Computer Science, The University of Western Australia, WA 6009, Australia. He is the recipient of an Australian Research Council Future Fellowship Award (project number FT210100268) funded by the Australian Government.

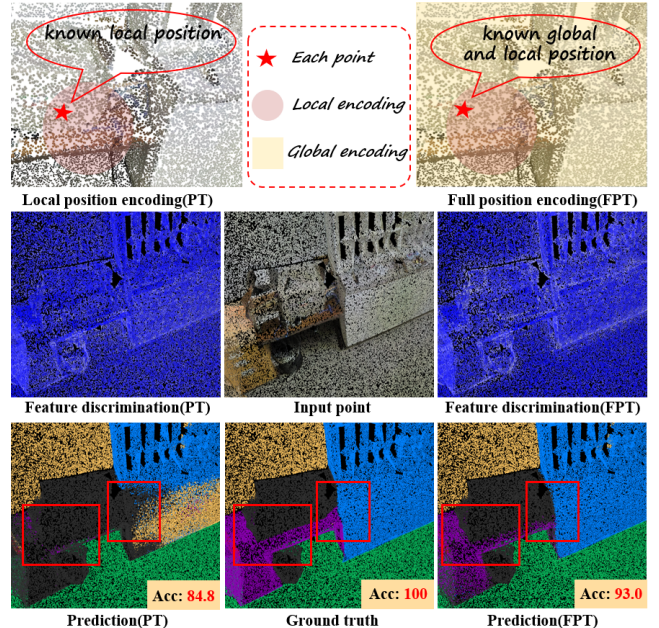


Fig. 1: Full point position encoding makes each point aware of its position in the global and local receptive field (top), helping the proposed FPTransformer to simultaneously model global and local geometric cues as well as their internal correlations. FPTransformer enhances discriminating features of long-range shapes, e.g. edges, improving the full shape awareness to achieve better semantic segmentation (see inside red boxes).

(MLPs) on each point and uses maxpooling to aggregate the features into a global representation. Such a design ignores local structures that are crucial for shape representation. To alleviate this problem, PointNet++ [11] additionally exploits local aggregation and adopts MLPs to learn local features. However, the local aggregator still treats the points independently, losing sight of the overall shape.

Inspired by 2D convolutions, some methods exploit point convolutions that learn the convolutional weights from local geometric connections. Early point convolutions use MLPs [12]–[16] as the convolutional weight function to learn weights from point coordinates. Other works approximate the weight functions as correlation functions [17]–[20]. Some methods associate coefficients (derived from point coordinates) [15], [16], [21] with weight functions to adjust the learned weights.

Self-attention was introduced to focus on important details in point clouds. Early methods in this category usually operate on global receptive field [22]–[27] and learn the attention maps through a scalar dot-product. Differently, point transformer [28] employs self-attention to local receptive field and uses

vector attention instead of scalar dot-product for learning the local geometric connections. Applying aggregation modules on local regions can effectively learn the local structure, but falls short of capturing the global context. To learn both local and global features, some methods integrate local and non-local feature aggregation modules into their network in a serial [26], [29] or parallel [27] manner. However, such pipelines still ignore the internal correlations between the local and global features besides significantly increasing the network parameters and leading to poor generalization.

We propose full point position encoding, applicable to convolution and transformer architectures. Specifically, we propose Full Point Convolution (FPCConv) and Full Point Transformer (FPTransformer) that exploit the local features and global context along with their interactions. FPCConv learns the local points layout in global receptive field by a global correlation function, and then learns the local points layout in local receptive field by a local correlation function, in a hierarchical manner. In FPTransformer, we introduce a novel position encoding scheme into the self attention that hierarchically encodes each point at the global and local level. This makes each point aware of its position in the global and local structure. Fig. 1 intuitively compares the local position encoding in Point Transformer [28] to full point position encoding in our FPTransformer. FPTransformer enhances the feature discrimination of long-range shapes (e.g. edges), improving the full shape awareness. In FPTransformer, we also propose a shape aware downsampling block which takes into account the local shape and the global context. Our contributions are summarized as follows:

- We derive a general formulation for local feature aggregation methods, including local point-wise MLP, point convolution and point transformer, to highlight their limitations.
- Based on the above general formulation, we propose a full point encoding method so as to simultaneously model local and global geometric features of point clouds along with their internal correlations. Using our novel encoding, we propose two network architectures, namely Full Point Convolution (FPCConv) and Full Point Transformer (FPTransformer) and show promising results with both.
- We propose a learnable downsampling block that performs local and global shape aware downsampling by incorporating the full point position encoding of the proposed FPTransformer into point-wise MLPs.

We conduct extensive experiments on benchmark datasets to show the efficacy of our proposed methods and their strong generalization ability to different tasks such as semantic segmentation, object detection, classification and normal estimation. FPCConv achieves competitive results on semantic segmentation, classification, and normal estimation tasks compared to various point convolution-based methods. FPTransformer achieves state-of-the-art semantic segmentation performance with 76.0% mIoU on S3DIS 6-fold and 72.2% mIoU on S3DIS Area 5. Incorporating FPTransformer into existing detection networks gives considerable performance improvement on ScanNetv2 and KITTI dataset.

II. RELATED WORK

Point-wise MLPs: To maximally preserve the geometric information, recent deep neural networks prefer to directly process raw point clouds. The pioneering work PointNet [10] uses shared MLPs to exploit point-wise features and adopts a symmetric function (i.e. maxpooling) to aggregate these features into global features. However, it fails to consider the geometric relationships of local points. PointNet++ [11] addresses this issue by adopting a hierarchical network that benefits from efficient sampling [16], [24], [27], [30], [31] and grouping [11], [26], [32]–[35] of the local region definition. However, MLP still treats each local point individually and ignores their geometric connections.

Follow up works construct geometric connections between points to enrich point-wise features and then apply shared MLPs on them. For instance, some methods [36], [37] hand craft the geometric connections through curves, triangles, umbrella orientation or affine transformation. Graphs are also used to connect local points [26], [38], [39] or global points [40]–[43], for subsequent geometric representation i.e. edge, contour, curvature, and connectivity. Although geometric connections do not largely increase the learnable network parameters, the parameters of these hand-crafted representations or graphs must be optimized for different datasets with varying density or shape style.

Point Convolution: Inspired by 2D convolutions, various works successfully proposed novel convolutions on points or their graphs that dynamically learn convolutional weights through functions that operate on the local geometric connections. Hence, the weight functions enable convolutions to be aware of the overall object shape. Early methods paid more attention to the weight function design. Most convolutional weight functions are approximated by MLP [12], [15], [16], [44], [45]. Other approaches treat weight functions as local correlation functions such as spline function [19], a family of polynomial functions [20], or standard unparameterized Fourier function [46] to learn the convolution weights from the local geometric connections.

Unlike the above dynamic convolution kernels, KPConv [18] and KCNet [17] fixed the convolution kernel for robustness to varying point density. These networks predefine the kernel points on local region and learn convolutional weights on the kernel points from their geometric connections to local points using linear and Gaussian correlation functions, respectively. Here, the number and position of kernel points need be optimized for different datasets.

Convolutional weights are generally learned from local geometric connections by weight functions. Hence, the convolutional weight learning highly depends on geometric connections. Some works construct additional low-level geometric connections (e.g. relative positions, 3D Euclidean distances [44], [45]) to enrich the input to the weight function. Another line of works [15], [16], [21] associate a coefficient (derived from point coordinates) with the weight function to adjust the learned convolutional weights. Convolutional weights learned from low-level geometric connections cannot embed the global context in the convolution operation. Besides, point cloud

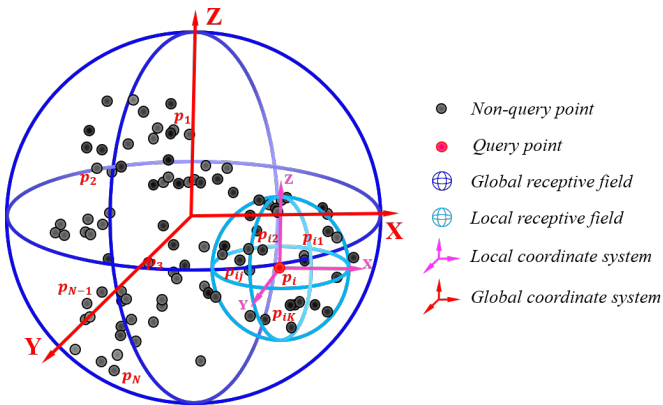


Fig. 2: Illustration of local and global receptive fields for a query point.

resolution decreases at deeper layers in many networks and the geometric connections constructed by the sparse points may get distorted, leading to non-robust weights learned by the weight function.

Point Transformer: Early self attention modules operate on global points [22]–[27] to learn the geometric point connections (i.e. attention map) through scalar dot-product. Such a pipeline suffers from high computational cost and struggles to learn large and complex 3D scenes. Point Transformer [28], [47], on the other hand, employs self-attention to local points and uses vector attention instead to construct the geometric connections between points. This not only requires fewer computations but helps the Point Transformer to learn robust attention weights from high-level geometric connections while encoding local point geometry. The success of Point Transformer shows the importance of point position encoding.

Applying the above local aggregation modules can learn the local structure well. However, the local regions divide the global scene into several sub-scenes, breaking the semantic continuity and integrity. Consequently, long-range features (e.g. line features) are not learned effectively because the local features aggregation module cannot exploit the global context. To address this issue, works [26], [27], [48] separately extract local features and global context by local and non-local aggregation, and then combine them in a serial and parallel manner. However, these approaches require enormous computations and are still unable to extract the inherent relationship between local features and global context. Motivated by these problems, we propose full point transformer, to simultaneously exploit local features, global context and their correlations.

III. METHOD

We revisit the three types of local point aggregations i.e., local point-wise MLP, point convolution and point transformer, and then derive a general formulation in Section III-A. Based on the general formulation, we present FPCConv in Section III-B and FPTransformer in Section III-C, followed by our down sampling block in Section III-D and finally, in Section III-E, we give our network details.

A. Rethinking Local Point Aggregation

Assume we have an unordered point cloud $\{p_i \mid i = 1, 2, \dots, N\} \in \mathbb{R}^{N \times 3}$ and its corresponding features $\{f_i \mid i = 1, 2, \dots, N\} \in \mathbb{R}^{N \times C}$. Here, p_i is a position vector and may also contain additional attributes such as color or surface normal. N and C are the number of points and feature channels respectively. We denote the K neighbors of p_i as $\{p_{ij} \mid j = 1, 2, \dots, K\} \in \mathbb{R}^{K \times 3}$ and their corresponding features are $\{f_{ij} \mid j = 1, 2, \dots, K\} \in \mathbb{R}^{K \times C}$, as illustrated in Fig. 2.

Local Point-wise MLP: The general formulation of local point-wise MLP on a point set p_i can be expressed as,

$$\mathcal{G}_i = \sum_{j=1}^K \text{MLP}(f_{ij}), \quad (1)$$

where MLP is a point-to-point mapping function that maps input features f_{ij} to output features \mathcal{G}_i . \sum is a symmetric function e.g. maxpool, sum. The input points have no communication between each other. To establish communication, some works use a function to construct geometric connections between points to enhance point-wise features and then employ an MLP on these enriched point-wise features

$$\mathcal{G}_i = \sum_{j=1}^K \text{MLP}(\mathcal{F}_1(p_{ij}, f_{ij})). \quad (2)$$

Here, $\mathcal{F}_1(\cdot)$ is as a geometric construction function (e.g. hand-crafted geometric descriptor, graph filter, MLP). These functions do not largely increase the network parameters, however, their parameters still need to be optimized, which impacts their ability to generalize across different datasets with varying point densities or shapes.

Local Point Convolution: Point convolutions introduce the weight function to convolutions such that it learns weights from local point coordinates to dynamically adjust the point-wise features, expressed as

$$\mathcal{G}_i = \sum_{j=1}^K \mathcal{W}(p_{ij}) f_{ij}, \quad (3)$$

where $\mathcal{W}(\cdot)$ is a weight function. Learning weights from the lowest level geometric information (i.e. point coordinates) may not lead to robust convolutional weights. Therefore, some works associate coefficients with weight functions that further adjust the learned weights. Others propose geometric construction functions that incorporate additional low-level geometric information (e.g. Euclidean distance, position difference, feature difference) to enrich the input to the weight functions, so that they can learn more robust convolutional weights. These are respectively expressed as,

$$\mathcal{G}_i = \sum_{j=1}^K \mathcal{C}(p_{ij}, f_{ij}) \mathcal{W}(p_{ij}) f_{ij}, \quad (4)$$

$$\mathcal{G}_i = \sum_{j=1}^K \mathcal{W}(\mathcal{F}_2(p_{ij}, f_{ij})) f_{ij}. \quad (5)$$

Here $\mathcal{C}(\cdot)$ is the coefficient (also derived from point coordinates or features) of weight function, and $\mathcal{F}_2(\cdot)$ is defined as a geometric construction function to construct the rich low level

geometric information, such as distance, coordinate difference, and feature difference.

The resolution of point cloud decreases at the deeper encoder layers in a hierarchical network leading to the distortion of low level geometric connections derived from sparse points. Learning convolutional weights from such distorted geometric information can lead to non-robust weights.

Local Point Transformer: Local point transformer solve the above problems and can be expressed as

$$\mathcal{G}_i = \sum_{j=1}^K \mathcal{W}(\mathcal{F}_2(p_{ij}, f_{ij}) + \delta(p_{ij}))(\mathcal{F}_1(p_{ij}, f_{ij}) + \delta(p_{ij})), \quad (6)$$

where $+$ is the addition operation, $\delta(\cdot)$ is the local position encoding that maps the point position in local coordinate system from low-dimension (3D) space to high dimension space. This makes each local point well aware of its position in the local shape. Observing the above formulations of the three classical local feature aggregation methods, we introduce a *general formulation* for local feature aggregation as

$$\mathcal{G}_i = \sum_{j=1}^K \mathcal{C}(p_{ij}, f_{ij}) \mathcal{W}(\mathcal{F}_2(p_{ij}, f_{ij}) + \delta(p_{ij})) (\mathcal{F}_1(p_{ij}, f_{ij}) + \delta(p_{ij})). \quad (7)$$

Although exiting local aggregation methods get promising performance on local point structures, they have two limitations, (1) they pay little to no attention to the global geometric structure, and (2) they completely ignore the internal connections between global and local structures.

B. Full Point Convolution

To exploit local features as well as the global context features along with their correlations, the Full Point Convolution (FPConv) is expressed as

$$\mathcal{G}(i) = \sum_{j=1}^K \mathcal{W}_c(\mathcal{S}_2(p_i, p_{ij}, \mathcal{S}_1(p_i, p_{in}))) f_{ij}, \quad (8)$$

where \mathcal{S}_1 and \mathcal{S}_2 denote the global and local correlation functions. \mathcal{W}_c is an adaptive weight function that learns the convolutional weights from local and global geometric connections.

Global Correlation Function: The goal of global correlation function is to construct the geometric connection between global points and local points, enriching the local points with global geometric information. We define the global correlation function as

$$\mathcal{S}_1(\cdot) = \sum_{n=1}^N \mathcal{R}(p_i, p_{in}), \quad (9)$$

where $\sum_{n=1}^N$ is the aggregation function implemented with summation. $\mathcal{R}(\cdot)$ is the relation between global point p_{in} and each point p_i , which should be higher when p_{in} is closer to p_i . Inspired by [18], we propose global linear relation function \mathcal{C}

$$\mathcal{R}(\cdot) = \max(0, 1 - \frac{\|p_i - p_{in}\|}{\sigma}), \quad (10)$$

where $\|\cdot\|$ is the Euclidean distance between global points and local points. σ is the influence coefficient that controls the influence of global points to each point. We set the correlation of global point to center point as \mathcal{S}_{1i} and its corresponding global correlation to neighborhood points as \mathcal{S}_{1ij} .

Local Correlation Function: Learning convolutional weights highly depends on the local geometric connections. Therefore, we construct sufficient geometric connections using a local connection function. We define the local correlation function as

$$\mathcal{S}_2(\cdot) = p_{ij} + (p_{ij} - p_i) + \|p_{ij} - p_i\| + (\mathcal{S}_{1i} - \mathcal{S}_{1ij}), \quad (11)$$

where p_i is the center point position, $p_{ij} - p_i$ is the position difference, $\|p_{ij} - p_i\|$ is the 3D Euclidean distance and $+$ denotes concatenation. Note that there is no learnable parameter in local and global correlation function, hence, they do not bring any computational overhead.

Efficient Weight Function: The goal of adaptive weight function $\mathcal{W}_c(\cdot)$ is to learn the kernel weights. The output of adaptive weight function are

$$\mathcal{W}_c = \rho_c(\phi_c(\mathcal{S}_2(p_i, p_{ij}, \mathcal{S}_1(p_i, p_{in})))), \quad (12)$$

where ϕ_c is implemented with Multi-layer Perceptrons (MLPs): $\mathbb{R}^{N \times K \times 8} \rightarrow \mathbb{R}^{N \times K \times C \times C}$ and ρ_c indicates softmax normalization. Learning a mount of weights from limited geometric connections $\in \mathbb{R}^{K \times 8}$ is inefficient. To this end, we formulate an efficient FPConv based on the following lemma.

Lemma: *FPConv is equivalent to the following formulation: $\mathcal{G} = \text{Max}(\mathcal{T}_{c2} \otimes \text{Conv}_{1 \times 1}(\mathcal{T}_{c1}, \mathcal{F}_c))$, where $\text{Conv}_{1 \times 1}$ is 1×1 convolution, \otimes is matrix multiplication and Max is maxpooling operation, $\mathcal{T}_{c1} \in \mathbb{R}^{C \times C_m \times C}$ is the kernels of 1×1 convolution, and $\mathcal{T}_{c2} \in \mathbb{R}^{K \times C_m}$ is the weight matrix learned by adaptive weight function.*

Proof: To better understand the FPConv reformulation, set attention weight matrix $\mathcal{W}_c \in \mathbb{R}^{N \times K \times C}$ as $\mathcal{W}_c(i, j, c) | i = 1, \dots, N, j = 1, \dots, K, c = 1, \dots, C$, and set $f_{ij} \in \mathbb{R}^{N \times K \times C}$ as $\mathcal{F}_c(i, j, c) | i = 1, \dots, N, j = 1, \dots, K, c = 1, \dots, C$, where i, j and c are the index of the global, neighbor points and input feature channels. According to Eq.8, FPConv can be expressed as

$$\mathcal{G}(i) = \sum_{j=1}^K \sum_{c=1}^C \mathcal{W}_c(i, j, c) \mathcal{F}_c(i, j, c). \quad (13)$$

Since the weight function is approximated by MLPs implemented as 1×1 convolutions, the weight matrix generated by weight function can be expressed as

$$\mathcal{W}_c(i, j, c_{in}) = \sum_{c_m=1}^{C_m} \mathcal{T}_{c2}(i, j, c_m) \mathcal{T}_{c1}^T(i, c, c_m), \quad (14)$$

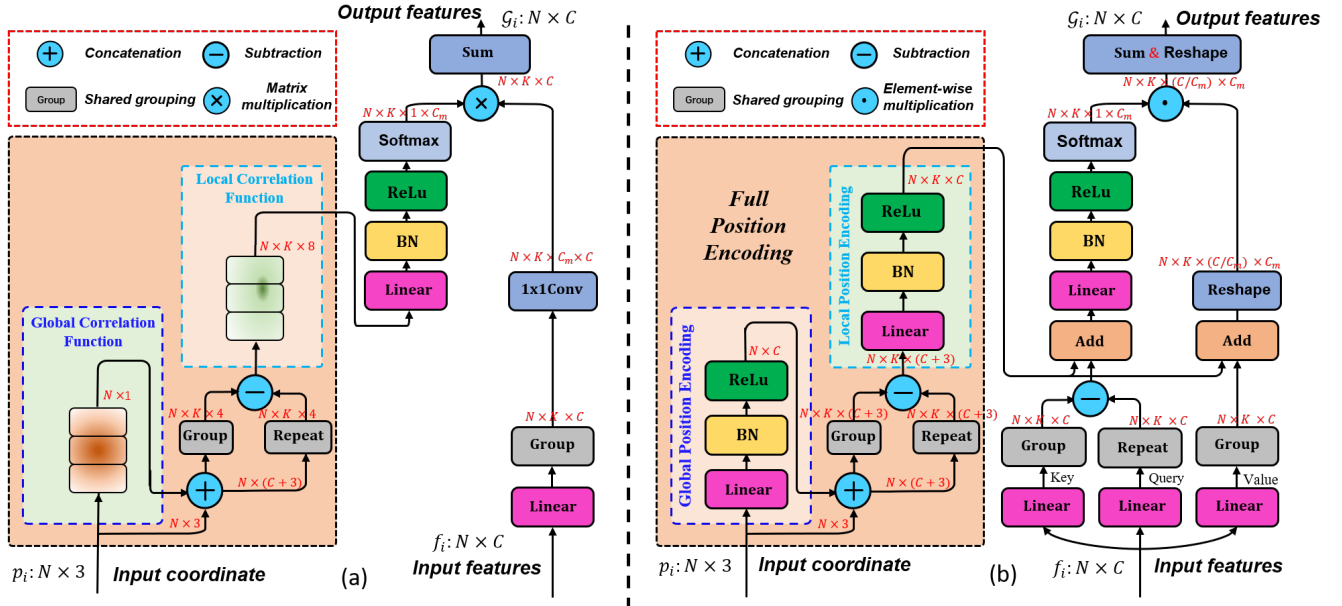


Fig. 3: (a) Proposed Full Point Convolution (FPConv) block which takes the $N \times 3$ input point coordinates and $N \times C$ features from the previous layer to output $N \times C$ features. FPConv incorporates full point correlation (global, local, and global-local correlation) into each point. (b) Proposed Full Point Transformer (FPTransformer) block which takes the $N \times 3$ input point coordinates and $N \times C$ features from the previous layer to output $N \times C$ features. FPTransformer incorporates full position encoding into each point.

where c_{mid} and C_{mid} are the index and number of output channels of the middle layer. Substituting Eq.14 into Eq.13, we get

$$\begin{aligned}
 \mathcal{G}(i) &= \sum_{j=1}^K \sum_{c=1}^C \mathcal{W}_c(i, j, c) \mathcal{F}_c(i, j, c) \\
 &= \sum_{j=1}^K \sum_{c=1}^C \left(\sum_{c_{mid}=1}^{C_m} \mathcal{T}_{c2}(i, j, c_{mid}) \mathcal{T}_{c1}^T(i, c, c_{mid}) \right) \mathcal{F}_c(i, j, c) \\
 &= \sum_{j=1}^K \sum_{c_m=1}^{C_m} \mathcal{T}_{c2}(i, j, c_m) \sum_{c=1}^C (\mathcal{T}_{c1}^T(c, c_{mid}) \mathcal{F}_c(i, j, c)) \\
 &= \text{Max}(\mathcal{T}_{c2} \otimes \text{Conv}_{1 \times 1}(\mathcal{T}_{c1}, \mathcal{F}_c)).
 \end{aligned} \quad (15)$$

According to the above reformulation, FPConv comprises three operations including one 1×1 convolution, one matrix multiplication and one maxpooling. Using this formulation, we divide the kernel weight matrix $\mathcal{W}_c \in \mathbb{R}^{N \times K \times C \times C}$ into two parts: 1×1 convolution weight matrix $\mathcal{T}_{c1} \in \mathbb{R}^{C \times (C_m \times C)}$ and weight matrix $\mathcal{T}_{c2} \in \mathbb{R}^{N \times K \times C_m}$, where the \mathcal{T}_{c1} are learned in data driven manner, and \mathcal{T}_{c2} are efficiently learned though the adaptive weight function according to the local and global geometric connections. Here the adaptive weight function can be defined as

$$\mathcal{T}_2 = \rho_{ce}(\phi_{ce}(\mathcal{S}_2(p_i, p_{ij}), \mathcal{S}_1(p_i, p_{in}))), \quad (16)$$

where ϕ_{ce} is a non-linear function implemented with Multi-layer Perceptrons (MLPs): $\mathbb{R}^{N \times K \times 8} \rightarrow \mathbb{R}^{N \times K \times C_m}$. ρ_{ce} indicates softmax normalization. The weight function transfers $K \times 8$ dimension geometric connection information to $N \times K \times C_m$ dimension weight matrix, where C_m is smaller than C . With the above reformulation, convolution can learn

more robust weights from limited geometric connections. Our reformulated FPConv is shown in Fig.3(a).

C. Full Point Transformer

We also bring this idea into point Transformer, we propose FPTransformer that exploits local features as well as the global context and their internal correlations. Give a point (p_i, f_i) , we use three linear projections to project the point features f_i to the query q_i , key k_i and value feature vectors v_i , expressed as

$$q_i = W_q f_i, \quad k_i = W_k f_i, \quad v_i = W_v f_i, \quad (17)$$

where W_q , W_k and W_v ($\mathbb{R}^{N \times C} \rightarrow \mathbb{R}^{N \times C}$) are projection functions implemented as linear layers. The FPTransformer applied on the point (p_i, f_i) and its corresponding point set (p_{ij}, f_{ij}) can be formulated as,

$$\mathcal{G}_i = \sum_{j=1}^K \mathcal{W}_a((q_i - k_{ij}) + \delta_{full}^a)(v_{ij} + \delta_{full}^a). \quad (18)$$

Here, \sum refers to an aggregation function such as summation, δ_{full}^a is the full position encoding for FPTransformer, and $\mathcal{W}_a(\cdot)$ is the Attention Function (i.e. Weight Function) that learns the attention map from the geometric connection between key point and query point.

Full Position Encoding: Point features are derived from their coordinates and already contain position information, however, this information may get diluted in deep aggregation layers. Therefore, we add fine-grained position information to features in each aggregation layer. Another limitation of existing position encoding methods is that they tend to map relative position in the local coordinate system from low

dimensional (3D) space to higher dimension. This enhances the awareness of local geometric connections but does not encode the global context. We propose full point position encoding that includes global and local position encoding. We define global position encoding on point $p_i \in \mathbb{R}^{N \times 3}$ as

$$\delta_{global,i}^a = [\phi_{global}^a(p_i), p_i], \quad (19)$$

the global position encoding function ϕ_{global}^a is an MLP: $\mathbb{R}^{N \times 3} \rightarrow \mathbb{R}^{N \times C}$. $[\cdot]$ is concatenation operation. The output of global position encoding is $\delta_{global,i}^a \in \mathbb{R}^{N \times (C+3)}$. we denote the neighborhood point position of $\delta_{global,i}^a$ as $\delta_{global,ij}^a | j = 1, 2, \dots, K$, where K is the number of neighborhood points. The full position encoding on local points $\delta_{global,ij}^a \in \mathbb{R}^{N \times K \times (C+3)}$ is defined as

$$\delta_{full}^a = \phi_{local}^a(\delta_{global,i}^a - \delta_{global,ij}^a), \quad (20)$$

where the local position encoding function ϕ_{local}^a is an MLP: $\mathbb{R}^{N \times K \times (C+3)} \rightarrow \mathbb{R}^{N \times K \times C}$. The output of full position encoding is $\delta_{full}^a \in \mathbb{R}^{N \times K \times C}$. With this hierarchical position encoding, each point perceives high dimensional position information in its global and local receptive fields.

Efficient Attention Function: Attention function plays an important role in our FPTransformer by encoding the geometric connections (i.e. features difference) between query and key points into the attention map. The attention function is formulated as

$$\mathcal{W}_a(\cdot) = \rho_a(\phi_a((q_i - k_{ij}) + \delta_{full}^a)), \quad (21)$$

where ϕ_a is an MLP ($\mathbb{R}^{N \times K \times C} \rightarrow \mathbb{R}^{N \times K \times C}$) and ρ_a is softmax normalization to keep the attention weights in the range (0,1). The attention function transfers $N \times K \times C$ geometric connection information to an attention weight matrix \mathcal{W}_a of same dimension. Since, the generation of attention weight matrix $\mathcal{W}_a \in \mathbb{R}^{N \times K \times C}$ requires large memory, we formulate an efficient attention layer as per the following lemma.

Lemma: *FPTransformer is equivalent to the following reformulation: $\mathcal{G}_i = \text{Sum}(\mathcal{T}_a \odot \mathcal{F}_a)$, where $\mathcal{T}_a \in \mathbb{R}^{N \times K \times 1 \times C_m}$ are the attention weights obtained from the attention function, $\mathcal{F}_a \in \mathbb{R}^{N \times K \times C/C_m \times C_m}$ is the reshaped feature. \odot is element-wise multiplication and Sum is summation.*

Proof: To better understand the FPTransformer reformulation, set attention weight matrix $\mathcal{W}_a \in \mathbb{R}^{N \times K \times C}$ as $\mathcal{W}_a(i, j, c) | i = 1, \dots, N, j = 1, \dots, K, c = 1, \dots, C$, and set $(v_{ij} + \delta_{full}^a) \in \mathbb{R}^{N \times K \times C}$ as $\mathcal{V}(i, j, c) | i = 1, \dots, N, j = 1, \dots, K, c = 1, \dots, C$, where i, j and c are the index of the global, neighbor points and input feature channels. As per to Eq.18, FPTransformer can be expressed as

$$\begin{aligned} \mathcal{G}_i &= \sum_{j=1}^K \sum_{c=1}^C \mathcal{W}_a(i, j, c) \odot \mathcal{V}(i, j, c), \\ &= \sum_{j=1}^K \sum_{c/c_m \times c_m=1}^{C/C_m \times C_m} \mathcal{W}_a(i, j, c/c_m \times c_m) \odot \mathcal{V}(i, j, c/c_m \times c_m), \\ &= \sum_{j=1}^K \sum_{c/c_m=1}^{C/C_m} \sum_{c_m=1}^{C_m} \mathcal{W}_a(i, j, c/c_m, c_m) \odot \mathcal{V}(i, j, c/c_m, c_m). \end{aligned} \quad (22)$$

Here, C_m is the number of middle channels ($C_m < C$), and c_m is the index of middle channel. We set $\{\mathcal{W}_a(i, j, 1, c_m) | i = 1, \dots, N, j = 1, \dots, K, c_m = 1, \dots, C_m\} \in \mathbb{R}^{C/C_m}$ as a vector from attention weight matrix $\mathcal{W}_a \in \mathbb{R}^{N \times K \times C/C_m \times C_m}$, and make these C/C_m number of vectors share the same attention weights. Hence, Eq.22 can be expressed as

$$\begin{aligned} \mathcal{G}_i &= \sum_{j=1}^K \sum_{c/c_m=1}^{C/C_m} \sum_{c_m=1}^{C_m} \mathcal{W}_a(i, j, c/c_m, c_m) \odot \mathcal{V}(i, j, c/c_m, c_m), \\ &= \sum_{j=1}^K \sum_{c/c_m=1}^{C/C_m} \sum_{c_m=1}^{C_m} \mathcal{W}_a(i, j, 1, c_m) \odot \mathcal{V}(i, j, c/c_m, c_m), \\ &= \text{Sum}(\mathcal{T}_a \odot \mathcal{F}_a). \end{aligned} \quad (23)$$

Here, $\mathcal{F}_a \in \mathbb{R}^{N \times K \times C/C_m \times C_m}$ is the reshaped feature. $\mathcal{T}_a \in \mathbb{R}^{N \times K \times 1 \times C_m}$ are the attention weights obtained from the efficient attention function defined as

$$\mathcal{W}_a(\cdot) = \rho_{ae}(\phi_{ae}((q_i - k_{ij}) + \delta_{full}^a)), \quad (24)$$

where ϕ_{ae} is an MLP ($\mathbb{R}^{N \times K \times C} \rightarrow \mathbb{R}^{N \times K \times C_m}$) and ρ_{ae} is softmax normalization. The attention function transfers $N \times K \times C$ dimensional geometric connection information to a $N \times K \times C_m$ dimensional attention weight matrix. Similarly, using this reformulation, transformer can learn more robust weights from limited geometric information. Details of C_m are further discussed in Section IV-E. Our reformulated FPTransformer is shown in Fig.3(b).

D. Shape-aware Downsampling (SADS) Block

A general downsampling block consists of one sampling and one grouping operation, however, downsampling decreases the resolution of the all points indiscriminately leading the loss of low-level geometric information. To overcome this problem, we propose a shape-aware downsampling (SADS) block with learnable parameters (see Fig. 4). SADS incorporates a low-level feature learner to maximally preserve the low-level features (i.e. shape details) of the scene. Our downsampling block can be expressed as

$$\mathcal{G}_i = \max(\text{MLP}(f_{ij} + H)), \quad (25)$$

where $f_{ij} \in \mathbb{R}^{M \times K \times C}$ are the features from grouping operation, M is the number of points sampled by Farthest Point Sampling (FPS), H are the hierarchical features of points (see Fig.4), and ‘max’ is maxpooling. The hierarchical features basically include low-level global and local features. The global features on point $p_i \in \mathbb{R}^{N \times 3}$ are learned by

$$f_{global,i}^d = [\phi_{global}^d(p_i), p_i], \quad (26)$$

where ϕ_{global}^d is an MLP: $\mathbb{R}^{N \times 3} \rightarrow \mathbb{R}^{N \times C}$. The low-level global features of wise point are $f_{global,i}^d \in \mathbb{R}^{N \times (C+3)}$. After sampling and grouping, we denote the neighborhood point position of sampled point $f_{global,i}^d \in \mathbb{R}^{M \times (C+3)}$ as $f_{global,ij}^d \in \mathbb{R}^{M \times K \times (C+3)}$. The hierarchical features H are defined as

$$H = \phi_{local}^d(f_{global,i}^d - f_{global,ij}^d), \quad (27)$$

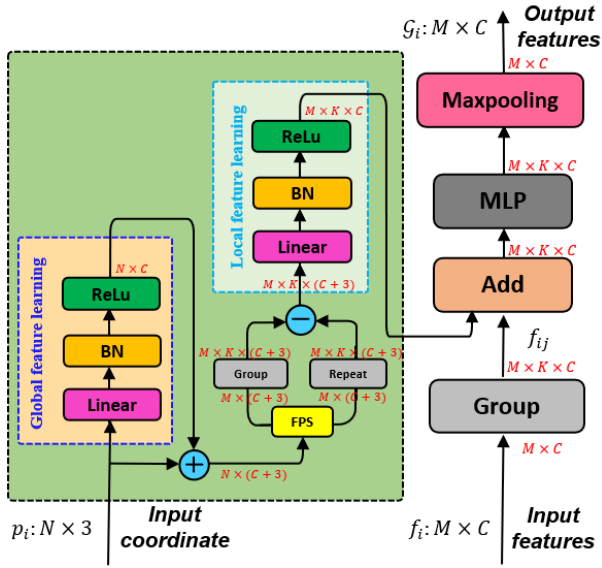


Fig. 4: Proposed Shape-aware Downsampling (SADS) block. Grouping is done based on the current features to which the full position encoding is added for subsequent downsampling.

where the local position encoding function is an MLP: $\mathbb{R}^{M \times K \times (C+3)} \rightarrow \mathbb{R}^{M \times K \times C}$. This way, simple but effective hierarchical MLPs are integrated into a conventional sampling block.

E. Network Architecture

For FPConv, we choose the basic PointNet++ [11] as the backbone, and replace the MLPs with FPConv to form the new network architectures for four tasks i.e. classification, normal estimation, and semantic segmentation.

For FPTransformer and SADS block, we use a U-Net like architecture with 5 encoding and decoding layers, and skip connections, covering semantic segmentation, 3D detection, and classification. The first encoding and decoding layers consist of one MLP and FPTransformer. Other encoding layers contain one SADS block and several FPTransformer blocks (details in Section IV). We set the feature dimensions C as [32,64,128,256,512] and middle feature dimension C_m as [4,8,16,32,64] for the 5 encoding and decoding layers. The ratio of up/down sampling is set as [1,4,4,4,4] for both encoder/decoder. Decoding layers, besides the first, contain one upsampling block and one FPTransformer. For segmentation, we add an MLP at the end to predict the final point-wise labels. For detection, we use the network as a 3D backbone (excluding the prediction layer).

IV. EXPERIMENTAL RESULTS

We evaluate our network on semantic segmentation, 3D detection, shape classification, and normal estimation tasks and perform detailed ablation studies to demonstrate the effectiveness and robustness of the proposed FPConv, FPTransformer and SADS.

A. Semantic Segmentation

Datasets: We evaluate our network on two large-scale indoor scene datasets, S3DIS and ScanNet. S3DIS [56] contains colored point clouds annotated point-wise with 13 classes. It covers 271 rooms from 6 large-scale indoor scenes (total of 6020 square meters). We conduct 6-fold cross validation on S3DIS and, in line with other works, conduct more extensive comparisons on Area 5 as the test set, which is not in the same building as the other areas. ScanNet [57] contains colored point clouds of indoor scenes with point-wise semantic labels of 20 object categories. It is split into 1201 scenes for training and 312 for validation.

Network Configuration: For semantic segmentation on S3DIS, we set the FPTransformer block in the 5 encoding layers depths [1,2,2,6,2]. We set the voxel size as 4cm and the maximum number of voxels to 80,000. We adopt the SGD optimizer and weight decay as 0.9 and 0.0001. The base learning rate is set as 0.5 and learning rate is scheduled by the MultiStepLR every 30 epochs. We train and test the model with batch size 16 on 4 GPUs and batch size 4 on a single GPU, respectively. We adopt scaling, contrast, translation, jitter and chromatic translation to augment training data. On ScanNet, we set the FPTransformer block in the 5 encoding layer depths as [1,3,9,3,3]. We set the voxel size as 2cm and the maximum number of voxels as 120,000. The base learning rate is set as 0.1. We use rotation, flip, scaling, and jitter to augment training data.

Results: We compare our method with the recent state-of-the-art on three metrics i.e. mean class-wise intersection over union (mIoU), mean overall accuracy (mAcc) and network parameters (Para.). Table I provides detailed results on S3DIS Area-5. Our network equipped with FPTransformer and shape-aware downsampling (SADS) achieves the best performance 72.2%, 78.5% and 91.5% in terms of mIoU, mAcc and OA, respectively. It also achieves competitive results (top 2) on 9 out of the 13 categories including *ceiling*, *floor*, *wall*, *column*, *window*, *door*, *table*, *board* and *clutter*. Moreover, compared to the classical vector attention based method (i.e. Point Transformer [28]), the performance of our method exceeds it by a large margin on some long-range shape classes such as *column*, *door*, *table*, *board*. Compared to the latest state-of-the-art network PointNeXt, our method not only outperforms it on mIoU and mAcc, but also has 74% less network parameters. Compared to the classical vector attention method (e.g. Point Transformer and Point Transformer V2), our FPTransformer gets significant improvements. Besides, our FPConv achieves the best performance among classical Convolution-based method such as KPConv and PAConv, and exceed the baseline PointNet++ 15% in the term of mIoU.

We report results in Table II for the 6-fold validation setting on S3DIS dataset. Our method again performs the best, achieving state-of-the-art results on all three metrics i.e. 76.0% mIoU, 84.0% mAcc and 91.0% OA. Notably, our method achieves the best performance on 9 out of the 13 categories and achieves the second best performance on another 2 categories. Fig. 5 shows visualizations of our results on S3DIS area 5 in comparison to Point Transformer. We can see that our method

TABLE I: Semantic segmentation results on S3DIS dataset Area-5. We report the mean class-wise intersection over union (mIoU), mean class-wise accuracy (mAcc) and overall accuracy (OA). The best result is in **Bold**, and second best is underlined.

Year	Method	mIoU	mAcc	OA	Para.	ceiling	floor	wall	beam	col.	wind.	door	chair	table	book	sofa	board	clut.
2017 CVPR	PointNet [10]	41.09	48.98	–	–	88.80	97.33	69.80	0.05	3.92	46.26	10.76	52.61	58.93	40.28	5.85	26.38	33.22
2018 NIPS	PointCNN [12]	57.26	63.86	85.9	–	92.3	98.2	79.4	0.0	17.6	22.8	62.1	74.4	80.6	31.7	66.7	62.1	56.7
2019 ICCV	KPConv [18]	67.1	72.8	–	–	92.8	97.3	82.4	0.0	23.9	58.0	69.0	91.0	81.5	75.3	<u>75.4</u>	66.7	58.9
2020 PAMI	SPH3D-GCN [49]	59.5	65.9	–	–	93.3	97.1	81.1	0.0	33.2	45.8	43.8	79.7	86.9	33.2	71.5	54.1	53.7
2020 CVPR	PointANSL [27]	62.6	68.5	87.7	22.4M	94.3	98.4	79.1	0.0	26.7	55.2	66.2	86.8	83.3	68.3	47.6	56.4	52.1
2020 CVPR	SegGCN [21]	63.6	70.4	–	–	93.7	<u>98.6</u>	80.6	0.0	28.5	42.6	74.5	80.9	88.7	69.0	71.3	44.4	54.3
2021 CVPR	PAConv [44]	66.58	73.00	–	–	<u>94.55</u>	<u>98.59</u>	82.37	0.00	26.43	57.96	59.96	<u>89.73</u>	80.44	74.32	69.80	73.50	57.72
2021 CVPR	BAAF-Net [50]	65.4	73.1	88.9	–	92.9	97.9	82.3	0.0	23.1	65.5	64.9	87.5	78.5	70.7	61.4	68.7	57.2
2022 CVPR	CBL [51]	69.4	75.2	90.6	–	93.9	98.4	84.2	0.0	37.0	57.7	71.9	81.8	<u>91.7</u>	75.6	77.8	69.1	62.9
2022 CVPR	RepSurf-U [36]	68.9	76.0	90.2	1M	–	–	–	–	–	–	–	–	–	–	–	–	–
2022 CVPR	Stratified Transformer [52]	<u>72.0</u>	<u>78.1</u>	91.5	–	–	–	–	–	–	–	–	–	–	–	–	–	–
2022 ECCV	PointMixer [53]	71.4	77.4	–	–	94.2	98.2	86.0	0.0	43.8	62.1	78.5	82.2	90.8	<u>79.8</u>	73.9	78.5	59.4
2022 NIPS	PointNeXt [54]	71.1	77.2	91.0	41.6M	94.2	98.5	84.4	0.0	37.7	59.3	74.0	91.6	83.1	<u>77.2</u>	77.4	<u>78.8</u>	60.6
2022 NIPS	Point Transformer V2 [47]	71.6	77.9	<u>91.1</u>	–	–	–	–	–	–	–	–	–	–	–	–	–	–
2018 NIPS	PointNet++ [11]	53.4	62.9	–	–	89.1	98.1	73.7	0.00	3.0	58.2	21.1	67.0	78.6	44.6	60.8	56.5	43.2
	FPConv(ours)	68.4(+15)	75.0(+12.1)	–	–	93.18	98.54	85.18	0.00	31.11	58.61	77.24	82.58	89.24	67.86	73.45	74.95	56.89
2021 ICCV	Point Transformer [28]	70.4	76.5	90.8	7.8M	94.0	98.5	<u>86.3</u>	0.0	38.0	63.4	74.3	82.4	89.1	80.2	74.3	76.0	59.3
	FPTransformer(ours)	72.2(+1.8)	78.5(+2.0)	91.5(+0.7)	10.9M	94.6	98.7	87.2	0.00	44.5	<u>64.8</u>	<u>77.0</u>	82.9	92.3	79.3	74.6	81.2	<u>61.8</u>

TABLE II: Semantic segmentation results on S3DIS with 6-fold cross validation. We report the mean class-wise IoU (mIoU), mean class-wise accuracy (mAcc) and overall accuracy (OA). Best result is in **Bold**, and second best is underlined.

Year	Method	mIoU	mAcc	OA	ceiling	floor	wall	beam	col.	wind.	door	chair	table	book	sofa	board	clut.
2017 CVPR	PointNet [10]	47.6	66.2	78.6	88.0	88.7	69.3	42.4	23.1	47.5	51.6	42.0	54.1	38.2	9.6	29.4	35.2
2018 NIPS	PointCNN [12]	65.4	75.6	88.1	<u>94.8</u>	97.3	75.8	63.3	51.7	58.4	57.2	69.1	71.6	61.2	39.1	52.2	58.6
2019 CVPR	PointWeb [38]	66.7	76.2	87.3	93.5	94.2	80.8	52.4	41.3	64.9	68.1	67.1	71.4	62.7	50.3	62.2	58.5
2019 ICCV	KPConv [18]	70.6	79.1	–	93.6	92.4	83.1	<u>63.9</u>	54.3	66.1	76.6	64.0	57.8	<u>74.9</u>	69.3	61.3	60.3
2020 PAMI	SPH3D-GCN [49]	68.9	77.9	88.6	93.3	96.2	81.9	58.6	55.9	55.9	71.7	<u>82.4</u>	72.1	64.5	48.5	54.8	60.4
2020 CVPR	PointANSL [27]	68.7	79.0	88.8	95.3	97.9	81.9	47.0	48.0	67.3	70.5	77.8	71.3	60.4	50.7	63.0	62.8
2020 CVPR	RandLA-Net [30]	70.0	82.0	88.0	93.1	96.1	80.6	62.4	48.0	64.4	69.4	76.4	69.4	64.2	60.0	65.9	60.1
2021 CVPR	PAConv [44]	69.31	78.65	–	94.30	93.46	82.80	56.88	45.74	65.21	74.90	59.74	74.60	67.41	61.78	65.79	58.36
2021 CVPR	SCF-Net [55]	71.6	82.7	88.4	93.3	96.4	80.9	64.9	47.4	64.5	70.1	81.6	71.4	64.4	67.2	<u>67.5</u>	60.9
2021 CVPR	BAAF-Net [50]	72.2	<u>83.1</u>	88.9	93.3	96.8	81.6	61.9	49.5	65.4	73.3	83.7	72.0	64.3	67.5	67.0	62.4
2022 NIPS	PointNeXt [54]	<u>74.9</u>	83.0	90.3	–	–	–	–	–	–	–	–	–	–	–	–	–
2022 CVPR	RepSurf-U [36]	74.3	82.6	<u>90.8</u>	–	–	–	–	–	–	–	–	–	–	–	–	–
2022 CVPR	CBL [51]	73.1	79.4	89.6	94.1	94.2	<u>85.5</u>	50.4	58.8	70.3	<u>78.3</u>	75.0	75.7	74.0	71.8	60.0	62.4
2021 ICCV	Point Transformer [28]	73.5	81.9	90.2	94.3	<u>97.5</u>	84.7	55.6	58.1	66.1	78.2	74.1	<u>77.6</u>	71.2	67.3	65.7	<u>64.8</u>
	FPTransformer(ours)	76.0(+2.5)	84.0(+2.1)	91.0(+0.8)	95.0	97.6	86.0	59.7	60.2	<u>68.3</u>	78.6	75.2	84.3	75.2	<u>69.6</u>	71.5	67.0

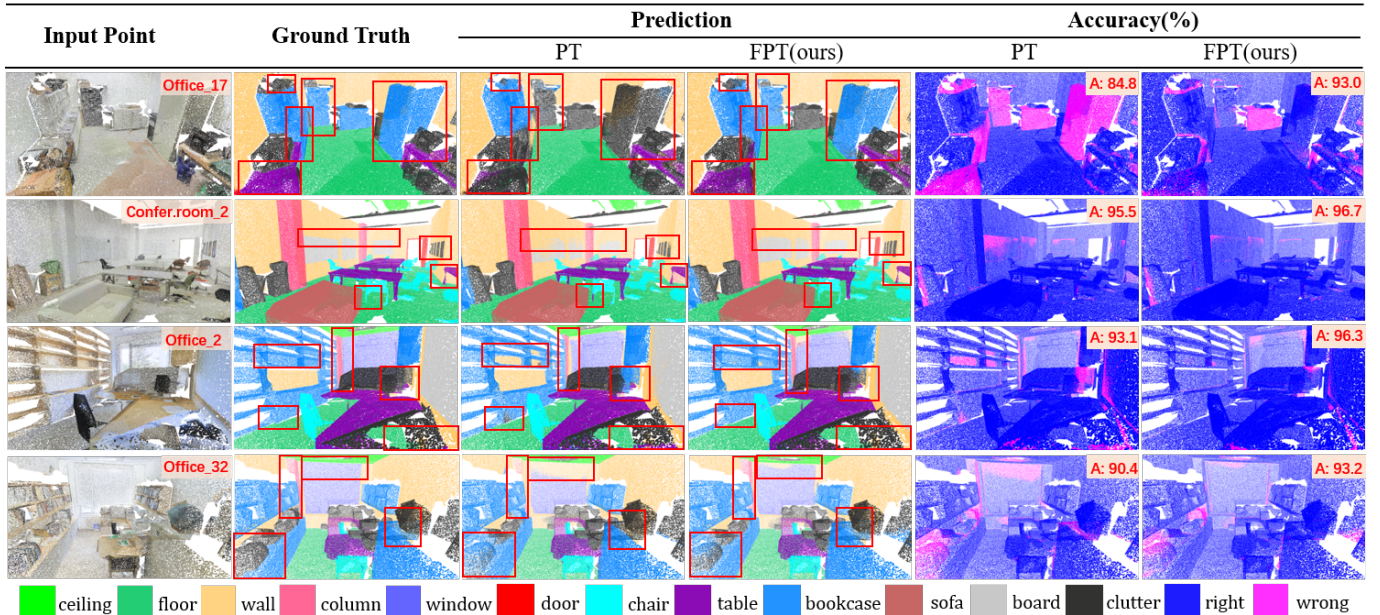


Fig. 5: Visualization of semantic segmentation results on S3DIS Area-5. The red boxes highlight areas in the scenes where our proposed FPTransformer performs particularly better than the Point Transformer (PT).

TABLE III: Semantic segmentation results (mIoU) on ScanNet Validation.

Year	Method	Input	#Parameter	mIoU(%)
2018 NIPS	PointNet++ [11]	point	–	53.5
2018 CVPR	SparseConvNet [58]	voxel	–	69.3
2019 CVPR	PointConv [15]	point	–	61.0
2020 CVPR	PointANSL [27]	point	–	63.5
2019 ICCV	MVPNet [59]	point	–	66.4
2019 ICCV	KPCConv [18]	point	14.9M	69.2
2019 3DV	JointPointBased [60]	point	–	69.2
2022 CVPR	RepSurf-U [36]	point	–	70.0
2022 CVPR	Stratified Transformer [52]	point	18.8M	74.3
2021 CVPR	BPNet [61]	point+image	–	72.5
2019 CVPR	MinkowshiNet [62]	voxel	37.9M	72.2
2022 CVPR	FastPointTransformer [63]	voxel	37.9M	72.0
2021 CVPR	PointTransformer [28]	point	10.7M	70.6
	FPTransformer (ours)	point	12.2M	73.9(+3.3)

is more robust to long-range shapes such as book case and board.

Table III shows semantic segmentation results on ScanNet validation set and compares the proposed FPTransformer to existing state-of-the-art. Compared to Point Transformer (which also uses vector attention), our method gets significant improvement of +3.3 in mIoU (Table III last row). Our method even outperforms the multi-modal BPNet [61]. Although our method performs slightly lower than Stratified Transformer, our network has about 35% fewer parameters. Compared to the popular voxel based methods FastPointTransformer [63] and MinkowshiNet [62], our method has higher mIoU and less than half the network parameters. In this experiment, our network used 2cm voxel size. More comparisons for varying voxel size are provided in the ablation study.

B. 3D Object Detection

We conduct experiments for 3D object detection to show the generalization ability of FPTransformer.

Datasets: We conduct experiments on two popular datasets: ScanNetV2 [57] and KITTI [64]. ScanNetV2 consists of 1513 indoor scenes and 18 object classes. On this dataset, we adopt mean Average Precision (mAP) metric under the threshold of 0.25 (mAP@0.25) and 0.5 (mAP@0.5) without considering the bounding box orientations. KITTI is a large scale outdoor dataset captured with LiDAR sensor. It has 7518 test and 7481 training samples (further divided into train-validation splits). We calculate mAP for easy, moderate, and hard cases, at 11 and 40 recall positions following the official KITTI protocol. **Network Configuration:** For ScanNetV2, we select two detection architectures: VoteNet [71] and Group-free-3D [72]. For KITTI, we choose PointRCNN [73] and PVRcnn [74]. VoteNet, Group-Free-3D and PointRCNN have a similar network architecture. They use a 3D backbone to extract point features for subsequent object bounding box prediction. We replace their 3D backbones with our network. PVRcnn integrates voxel and point features, where the voxel features are learned by 3D sparse convolution using multiple encoding layers and summarized into a small set of key points via the voxel set abstraction module. We replace the abstraction module with our FPTransformer. During training, we keep the

TABLE IV: Detection results on ScanNetV2 validation set from the benchmark website. We report mAP at thresholds of 0.25 and 0.5 IoU. * denotes model reproduced by [65].

Year	Method	3D Backbone	mAP0.25	mAP0.5
2020 ECCV	H3DNet [66]	4×PointNet++	67.2	48.1
2021 ICCV	3DETR [67]	Transformer	65.0	47.0
2021 CVPR	BRNet [68]	4×PointNet++	66.1	50.9
2022 CVPR	TokenFusion [69]	2×PointNet++	70.8	54.2
2022 CVPR	RBGNet [70]	PointNet++	70.6	55.2
2022 CVPR	RepSurf-U [36]	PointNet++	71.2	54.8
2019 CVPR	VoteNet [71]	PointNet++	58.6	33.5
	VoteNet (ours)	FPTransformer	62.3(+3.7)	38.6(+5.5)
2019 CVPR	VoteNet* [71]	PointNet++	62.9	39.9
	VoteNet* (ours)	FPTransformer	65.2(+2.3)	45.1(+5.2)
2021 CVPR	Group-Free-3D(6,256) [72]	PointNet++	67.3	48.9
	Group-Free-3D(6,256) (ours)	FPTransformer	69.2(+1.9)	50.7(+1.8)
2021 CVPR	Group-Free-3D(12,512) [72]	2×PointNet++	69.1	52.8
	Group-Free-3D(12,512)(ours)	FPTransformer	71.5(+2.4)	54.3(+1.5)

same parameters of the original PointRCNN and PVRcnn networks. However, for VoteNet, we change the number of input points to 40,960 and epochs to 260. For Group-Free-3D, we only adopt the point coordinates as input features.

Results: As shown in Table IV, when FPTransformer is plugged into the VoteNet and Group-Free-3D networks, the detection performance improves significantly on ScanNetV2. Specifically, VoteNet official model with FPTransformer obtains 3.7% mAP@0.25 and 5.5% mAP@0.5 improvements. Similarly, the VoteNet reproduced by [65] with FPTransformer obtains 2.3% mAP@0.25 and 5.2% mAP@0.5 improvements on the MMDetection3D platform. As shown in Figure 6, FPTransformer helps VoteNet to reduce false positive detection. Our FPTransformer backbone also improves the accuracy of both versions of the the Group-Free-3D detection network. Specifically, the Group-Free-3D (12 decoder layers, 512 object candidates) with our FPTransformer backbone gains 2.4% mAP@0.25 and 1.5% mAP@0.5 improvement, outperforming all prior models equipped with transformer modules such as 3DETR [67] and TokenFusion [69], on the mAP@0.25 metric.

Table V shows results on the KITTI dataset. Our method consistently improves the performance of both detectors for Recall@40 and improves 13 out of 18 cases for Recall@11. PointRCNN with FPTransformer obtains remarkable improvements of 5.75%, 6.57%, 7.34% (Recall@40) on the easy, moderate, hard cases of the ‘Pedestrian’ class. PVRcnn with FPTransformer obtains significant improvements of 1.77%, 3.29% for the hard cases of ‘Pedestrian’, ‘Cyclist’.

C. Classification

Synthetic Data: We firstly evaluate FPConv and FPTransformer on ModelNet40 [75] which comprises 12,311 CAD models from 40 categories. The data is divided into 9,843 training and 2,468 test models. We uniformly sample 1024 points from each models and only use their (x, y, z) coordinates as input. The training data is augmented by randomly translating in the range $[-0.2, 0.2]$, scaling in the range $[0.67, 1.5]$.

Real-world Data: We also evaluate our network on the real-world ScanObjectNN dataset [76] which includes 15,000

TABLE V: 3D object detection results on the KITTI validation set. We report mean Average Precision (mAP) at 11 and 40 recall positions, similar to prior works [73], [74].

Methods	3D Backbone	Car(%)			Pedestrian(%)			Cyclist(%)			Recall
		Easy	Moderate	Hard	Easy	Moderate	Hard	Easy	Moderate	Hard	
PointRCNN [73]	PN++(MSG)	88.72	78.55	77.72	62.64	55.06	50.83	85.68	71.22	65.63	R@11
PointRCNN [73]	PT	88.89	78.62	77.94	65.53	58.24	55.76	83.95	69.45	64.97	
PointRCNN(ours)	FPTrans.	89.05(+0.33)	78.89(+0.44)	78.44(+0.72)	68.78(+6.14)	61.45(+6.39)	56.57(+5.74)	84.10(-1.58)	70.15(-1.07)	65.55(-0.08)	
PV-RCNN [74]	Spconv + MLP	89.23	83.23	78.81	67.29	61.01	56.40	87.16	73.45	68.98	
PV-RCNN [74]	Spconv + PT	89.10	82.98	77.76	67.75	61.20	56.43	86.64	72.54	69.11	
PV-RCNN (ours)	Spconv + FPTrans.	89.43(+0.2)	83.60(+0.37)	78.84(+0.03)	68.21(+0.92)	61.45(+0.44)	56.62(+0.22)	86.59(-0.57)	72.32(-1.13)	69.27(+0.29)	
PointRCNN [73]	PN++(MSG)	91.28	80.47	78.02	62.80	55.41	48.83	90.58	70.98	66.65	R@40
PointRCNN [73]	PT	91.10	80.23	77.96	65.74	58.65	53.45	90.68	71.04	66.84	
PointRCNN (ours)	FPTrans.	91.30(+0.02)	81.87(+1.40)	80.14(+2.12)	68.55(+5.75)	61.98(+6.57)	56.17(+7.34)	91.76(+1.18)	71.45(+0.57)	67.24(+0.59)	
PV-RCNN [74]	Spconv + MLP	92.00	84.38	82.42	68.19	60.55	55.55	90.39	70.38	65.97	
PV-RCNN [74]	Spconv + PT	92.04	84.45	82.43	68.23	60.76	56.23	91.45	71.23	67.56	
PV-RCNN (ours)	Spconv + FPTrans.	92.15(+0.15)	84.74(+0.36)	82.62(+0.20)	68.24(+0.05)	61.10(+0.55)	57.32(+1.77)	92.71(+2.32)	72.50(+2.12)	69.26(+3.29)	

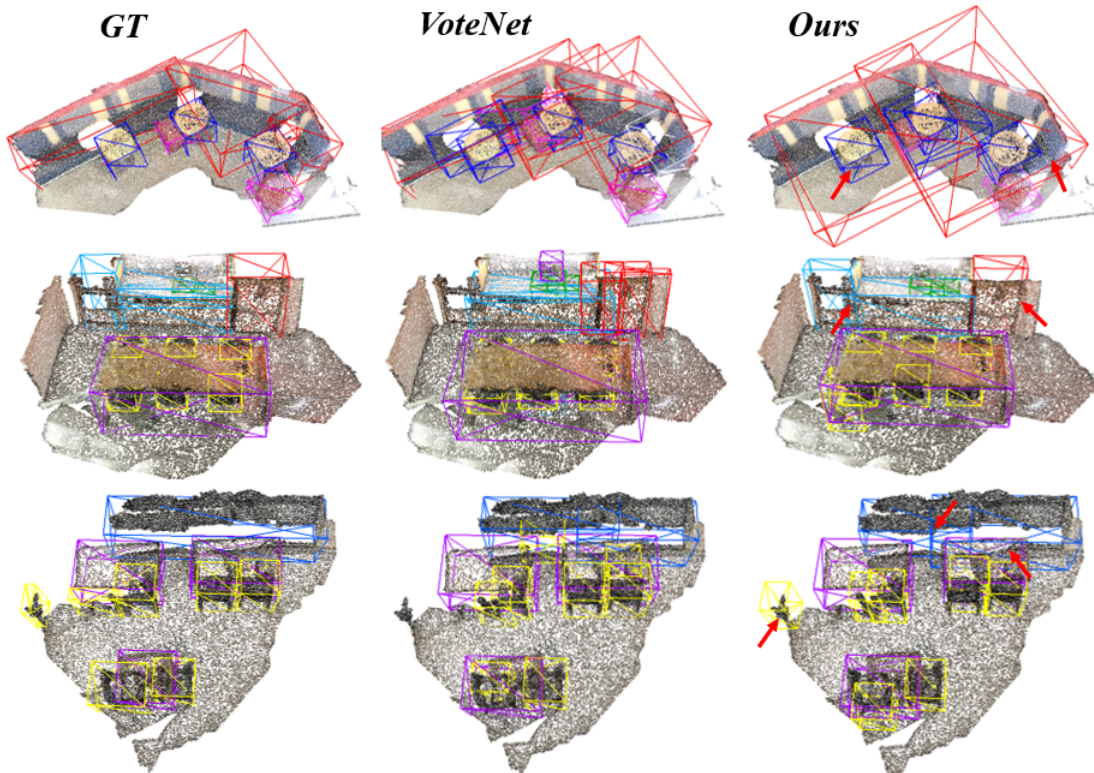


Fig. 6: Visualization of detection results on ScanNetV2. The red arrows indicate objects in the scenes where the VoteNet equipped with FPTransformer performs better than original VoteNet.

objects categorized into 15 classes. Unlike the synthetic ModelNet40 objects, these objects are with occlusion, background noise, deformed geometric shapes and non-uniform surface density providing a more challenging scenario. We conduct experiments on its hardest perturbed variant (i.e. PB_T50_RS variant). We uniformly sample 1024 points from each object and only use their (x, y, z) coordinates as input. The training data is augmented similar to ModelNet40.

Network Configuration: We use the same network configuration for ModelNet40 and ScanObjectNN. During training, we use SGD optimizer with 0.9 momentum and 0.1 initial learning rate to train our model for 350 epochs with a batch size of 32. We adopt cosine annealing to dynamically adjust the learning rate when it drops to 0.001 and use a dropout ratio of 0.4.

Results: We compare our method with representative state-of-

the-art methods in Table VI using the overall accuracy (OA) metric. For better comparison, we also show input data type and number of input points for each method. The FPConv network achieves competitive OA of 93.9% on ModelNet40 and 85.6% on ScanObjectNN, giving significant improvements of 3.2% and 7.7% over the backbone PointNet++ [11]. On ModelNet40, our network outperforms the classical local point convolution KPConv [18], by 1% even though KPConv uses 7,000 input points and our network only uses 1,024 points. Moreover, our network outperforms RS-CNN when voting strategy is not used.

The FPTransformer network achieves the state-of-the-art OA of 94.1% on ModelNet40 and 86.0% on ScanObjectNN. On ModelNet40, our network outperforms vector attention based method (e.g. Point Transformer) by 0.4% and scalar attention based method (e.g. PointANSL) by 0.9%, even

TABLE VI: Classification results on ModelNet40 and ScanObjectNN dataset. Our network achieves the best overall accuracy. ‘xyz’ and ‘n’ represent coordinates and normal vector. ‘K’ stands for one thousand. ‘PN++’ stands for PointNet++ and ‘*’ denotes methods evaluated with voting strategy [45].

Method	Input	#Points	OA(%)	
			ModelNet40	ScanObjectNN
PointWeb [38]	xyz, n	1K	92.3	-
PointConv [15]	xyz, n	1K	92.5	-
SpiderCNN [20]	xyz, n	5K	92.4	-
KPConv [18]	xyz	7K	92.9	-
PointASNL [27]	xyz, n	1K	93.2	-
PRANet [29]	xyz	2K	93.7	<u>82.1</u>
RS-CNN [45]	xyz	1K	92.9	-
RS-CNN* [45]	xyz	1K	93.6	-
3DmFV [77]	xyz	1K	91.4	63.0
PointNet [10]	xyz	1K	89.2	68.2
PointNet++ [11]	xyz	1K	90.7	77.9
DGCNN [41]	xyz	1K	92.9	78.2
PointCNN [12]	xyz	1K	92.2	78.5
BGA-DGCN [76]	xyz	1K	-	79.9
BGA-PN++ [76]	xyz	1K	-	80.2
DRNet [78]	xyz	1K	93.1	80.3
GBNet [79]	xyz	1K	93.8	80.5
PointASNL [27]	xyz	1K	92.9	-
PRANet [29]	xyz	1K	93.2	81.0
PointNet++ [11]	xyz	1K	90.7	77.9
FPConv(ours)	xyz	1K	93.6 (+2.9)	84.6 (+6.7)
FPConv*(ours)	xyz	1K	<u>93.9 (+3.2)</u>	<u>85.6 (+7.7)</u>
PointTransformer [28]	xyz	1K	93.7	-
FPTransformer(ours)	xyz	1K	94.1(+0.4)	86.0

though PointASNL additionally uses surface normals as input. On ScanObjectNN, our network gets the highest accuracy of 86.0%, outperforming all methods by a large margin. Remarkably, our network exceeds the state-of-the-art PRANet by 4.9% with the same number of input points. Superior performance on real-world datasets indicates that our method is more suitable for practical applications.

D. Normal Estimation

Data: Surface normal estimation in point clouds is significant to 3D reconstruction and rendering. We take normal estimation as a supervised regression task, and use the semantic segmentation architecture to achieve it. We conduct the experiment on the ModelNet40 [75], where each point is labeled with its three-directional normal. During training, we uniformly sample 1024 points from each model and only use their (x, y, z) coordinates as input.

Network Configuration: The normal estimation network has a similar architecture to the semantic segmentation network apart from the final softmax layer. The K nearest neighborhood in encoding layers is set to 16. We use the SGD optimizer with 0.9 momentum and 0.05 initial learning rate to train our network for 200 epochs with a batch size of 32. The cosine annealing starts to dynamically adjust the learning rate when it drops to 0.0005.

Results: Table VII summarizes our normal estimation results. FPConv achieves the competitive performance with a error of 0.12. It reduces the error of the backbone PointNet++ [11] by 58.6% and reduces the error compared to prior state-of-the-art RS-CNN [45] by 20%. FPTransformer achieve the state-of-the-art performance with a minimum error of 0.10.

TABLE VII: Normal estimation results on ModelNet40. ‘xyz’ represents coordinates and ‘K’ stands for thousand.

Method	Input	#Point	Error
PointNet [10]	xyz	1K	0.47
PointNet++ [11]	xyz	1K	0.29
DGCNN [41]	xyz	1K	0.29
PCNN [80]	xyz	1K	0.19
RS-CNN [45]	xyz	1K	0.15
FPConv(ours)	xyz	1K	<u>0.12</u>
FPTransformer(ours)	xyz	1K	0.10

E. Ablation Studies

We conduct ablation studies to demonstrate the effectiveness of FPTransformer and SADS block. The first three ablation experiments are performed on S3DIS Area 5 [56], the fourth and fifth ablation experiment is performed on ScanNet [57] (segmentation dataset). We conduct the last ablation study on ScanObjectNN [76] and S3DIS [56] to determine the optimal coefficient σ in FPConv.

Position Encoding. We study the effects of different encoding strategies used for the position encoding in our Transformer encoder. We compare the proposed full position encoding (FPE) with some classical position encoding strategies such as local position encoding (LPE) and global position encoding (GPE). For each of the three cases, we test with learnable MLP or nonlearnable Sinusoidal [81] position encoding. The results are shown in Table VIII. We can see that the performance of global position encoding is lower than that of local position encoding. The underlying cause is that global position encoding lacks the geometric connection information. When full position encoding strategy is incorporated into the Transformer, the network achieves the highest performance. Our results also show that the MLP encoder is more flexible than Sinusoidal encoder. This indicates our proposed point transformer with full position encoding has more geometric awareness.

TABLE VIII: Segmentation performance of our model on S3DIS area 5 with different position encoding. LPE: local position encoding, GPE: global position encoding, FGE: proposed full position encoding. MLP: MLP encoder, Sinusoidal: sinusoidal encoder. The network does not include SADS block.

Encoder	Strategy	mIoU(%)	Encoder	Strategy	mIoU(%)
Sinusoidal	LPE	69.8	MLP	LPE	70.2
Sinusoidal	GPE	68.4	MLP	GPE	69.3
Sinusoidal	FPE	70.5	MLP	FPE	71.5

Efficient Attention. We study the effect of middle channel numbers in our efficient attention function. For this, we test four cases in encoding and decoding layers. Table IX compares the mIoU, mAcc, OA, and network parameters (Para.) of different cases. As we can see, the difference in the number of parameters is not much but when the number of middle channels are set as [4, 8, 16, 32, 64], the network gets the best results on all three metrics. More middle channel numbers slightly increase network parameters and the network can not find a good local optimum with limited training. Conversely, less middle channel numbers weakens the geometric encoding ability of the Transformer. Overall, the performance of the

TABLE IX: Ablation study on the number C_m of middle channels in efficient attention function. ‘M’ means million.

case	C_m	mIoU(%)	mAcc(%)	OA(%)	Para.
1	[8, 16, 32, 64, 128]	70.7	77.5	90.8	11.1M
2	[4, 8, 16, 32, 64]	72.2	78.5	91.5	10.9M
3	[2, 4, 8, 16, 32]	70.2	77.4	91.3	10.7M
4	[8, 8, 16, 16, 32]	70.8	77.0	90.8	10.7M

network remains stable, even for large variations in the channel numbers.

Sampling Block. To prove the effectiveness of our proposed shape-aware downsampling (SADS) block, we compare it with two types of downsampling blocks including the baseline general downsampling block (GDS) and the transition downsampling block (TDS) [28]. GDS consists of one sampling, one grouping and maxpooling operation. Table X shows the performance of our network with different sampling blocks. Compared to the TDS, the network integrated with SADS block gets a higher improvement (+ 3%, + 2.2%, + 1.2%) in terms of mIoU, mAcc, and OA with only a minor increase in parameters (+ 0.4M).

TABLE X: Ablation study for different sampling blocks. Δ stands for the difference. ‘M’ means million.

Sampling Block	mIoU	$\Delta mIoU$	mAcc	$\Delta mAcc$	OA	ΔOA	Para	$\Delta Para$
GDS	69.2	–	76.3	–	89.3	–	10.5M	–
TDS	71.5	+2.3	78.2	+1.9	91.1	+0.8	10.7M	+0.2M
SADS (ours)	72.2	+3.0	78.5	+2.2	91.5	+1.2	10.9M	+0.4M

Voxel Size. We conduct experiments on the ScanNet dataset with different voxel size (i.e. 5cm and 2cm). For a fair comparison, we use the transition downsampling block [28] instead of SADS block. Table XI shows that the performance of our FPTransformer exceeds that of the Point Transformer [28] and MinkowshiNet [62] by a large margin in terms of mIoU. With the 2cm voxel size, our FPTransformer not only gets a better performance (+0.6%) than Fast Point Transformer, but also has 25.9M less parameters. Especially, our method (while using only one modality) can keep a similar performance with the multi-modal method BPNet [61].

Neighborhood Point. Table XII provides detection results of VoteNet [71] integrated with FPTransformer for the different number of neighborhood points. We use the ScanNetV2

TABLE XI: Ablation study for voxel size. We perform semantic segmentation on ScanNet Validation. Note that the network excludes the SADS block.

Year	Method	Input	#Para(M)	mIoU(%)
<i>voxel/grid size: 5cm</i>				
2019 CVPR	MinkowshiNet [62]	voxel	37.9	66.6
2021 CVPR	BPNet [61]	point+image	–	70.6
2021 CVPR	PointTransformer [28]	point	10.7	68.0
2022 CVPR	FastPointTransformer [63]	voxel	37.9	70.1
	FPTransformer(ours)	point	12.0	70.0
<i>voxel/grid size: 2cm</i>				
2019 CVPR	MinkowshiNet [62]	voxel	37.9	72.2
2021 CVPR	BPNet [61]	point+image	–	72.5
2021 CVPR	PointTransformer [28]	point	10.7	70.6
2022 CVPR	FastPointTransformer [63]	voxel	37.9	72.0
	FPTransformer(ours)	point	12.0	72.6

TABLE XII: Ablation study for object detection on ScanNetV2 using different number of neighborhood points.

case	Neighborhood points	mAP@0.25	mAP@0.5
1	[8,64,16,16,16]	60.72	37.71
2	[8,64,32,16,16]	59.41	37.72
3	[8,32,16,16,16]	62.15	38.87
4	[8,32,8,8,8]	59.23	36.32
5	[8,28,8,8,8]	62.31	38.58
6	[8,24,8,8,8]	59.30	37.02

dataset for this experiment and reproduce VoteNet using its official code as well as integrate the FPTransformer into it. As we can see, when the neighborhood points are set as [8,28,8,8,8], the network achieves the best performance of 62.31% on the mAP@0.25 metric and when the neighborhood points are set as [8,32,16,16,16], the network gets the best performance of 38.87% on the mAP@0.5 metric.

Coefficient σ : We vary the coefficient σ and observe the performance of our network on ScanObjectNN and S3DIS datasets. As shown in Table XIII, our network is not sensitive to the choice of σ and the best performance is achieved on ScanObjectNN and S3DIS with coefficient 1.2 and 0.2 respectively.

TABLE XIII: Classification and semantic segmentation results of FPConv with different influence coefficient σ .

σ	ScanObjectNN(OA%)	σ	S3DIS(mIoU%)
0.8	84.07	0.1	64.98
1.0	84.39	0.2	66.80
1.2	84.60	0.4	66.71
1.4	83.48	0.6	64.78
1.6	83.41	0.8	65.89

F. Robustness Analysis

Robustness to Density: We compare the robustness of our models to point density with several typical baselines such as PointNet [10], PointNet++ [11], DGCNN [41], as well as classical convolutional network such as RS-CNN [45], PointASNL [27]. For a fair comparison, all the networks are trained on modelnet40_normal_resampled dataset [75] with 1024 points using only coordinates as the input. During test, we use downsampled points of 1024, 512, 256, 128, 64 as input to the trained model. Results are shown in Fig. 7. As the input points get sparse, the classification accuracy of all networks drops. Overall, our FPConv and FPTransformer remain more robust than other networks.

Robustness to Transformation: To demonstrate the robustness of our FPTransformer, we evaluate its performance on S3DIS under a variety of perturbations in the test data, including permutation, translation, scaling and jitter. As shown in Table XIV (top), our method’s performance remains extremely stable under various transformations. Specially, the performance even improves (+0.21%, +0.27% and +0.10% mIoU) under the -0.2 translation in x, y, z axis, and $\times 1.2$ scaling and jitter.

We further evaluate the transformation robustness of our FPConv on ModelNet40 at test time. Table XIV (bottom) shows that all methods are invariant to permutations. In terms

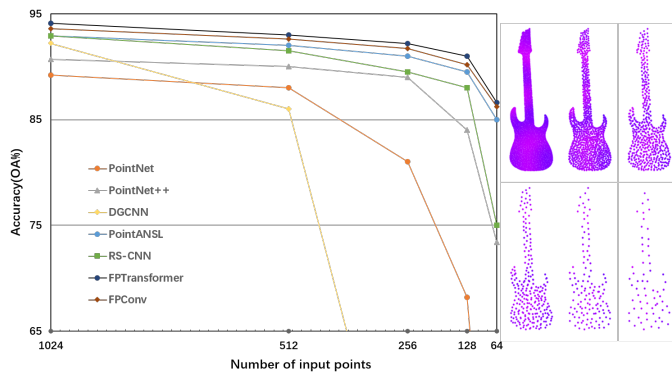


Fig. 7: FPConv shows the highest robustness to decreasing density of input points. All models were trained with 1024 points. An example guitar is shown for illustration.

of sensitivity to point scaling, FPConv performs relatively better when the scaling range is decreased. FPConv achieves the best accuracy under all transformations.

TABLE XIV: Robustness study for random point permutations, translation of ± 0.2 in x, y, z axis, scaling ($\times 0.8, \times 1.2$) and jittering. FPTransformer and FPConv achieve the best results under all transformations.

Methods	None	Perm.	Translation		Scaling		Jitter
			+ 0.2	- 0.2	$\times 0.8$	$\times 1.2$	
S3DIS Dataset mIoU(%)							
PointNet [66]	57.75	59.71	22.33	29.85	56.24	59.74	59.04
MinKowshi [82]	64.68	64.56	64.59	64.96	59.60	61.93	58.96
PAConv [68]	65.63	65.64	55.81	57.42	64.20	63.94	65.12
PT [28]	70.36	70.45	70.44	70.43	65.73	66.15	59.67
STrans. [52]	71.96	72.02	71.99	71.93	70.42	71.21	72.02
FPTransformer(ours)	72.21	72.23	72.31	72.42	72.09	71.48	72.31
ModelNet40 Dataset OA(%)							
PointNet++ [11]	92.1	92.1	90.7	90.8	91.2	91.0	91.0
DGCNN [41]	92.5	92.5	92.3	92.3	92.1	92.3	91.5
PointConv [15]	91.8	91.8	91.8	91.8	89.9	90.6	90.6
FPConv(ours)	93.6	93.6	93.5	93.5	92.4	92.8	91.6

Robustness to Noise: To verify the robustness of FPConv and FPTransformer to noise, we conduct experiments the PB_T50_RS variant with background noise ('obj_bg') and without background noise ('obj_nobg') of ScanObjectNN. Table XV compares the results of our models with some baselines provided in [76]. The overall accuracy of all networks decreases when trained and tested in the presence of background noise. However, our model gets the highest accuracy and the lowest performance drops 0.7% and 1.6% from 'obj_nobg' variant to 'obj_bg' variant, outperforming all compared networks by a large margin.

V. CONCLUSION

We proposed a novel full point encoding method to simultaneously explore the local and global features of point clouds as well as their internal correlations. Using the proposed encoding, we designed FPConv and FPTransformer and evaluated their performance on various tasks such as semantic segmentation, 3D detection, classification and normal estimation. Extensive experiments on challenging benchmarks, as well as thorough ablation studies and theoretical analysis

TABLE XV: Robustness to background noise on ScanObjectNN without voting strategy [45]. 'obj_bg', 'obj_nobg' stand for objects with and without background noise.

Method	obj_nobg	obj_bg	OA drop(%)
3DmFV [77]	69.8	63.0	6.8↓
PointNet [10]	74.4	68.2	6.2↓
PointNet++ [11]	80.2	77.9	2.3↓
SpiderCNN [20]	76.9	73.7	3.2↓
DGCNN [15]	81.5	78.1	3.4↓
PointCNN [12]	80.8	78.5	2.3↓
FPConv	85.3	84.6	0.7↓
FPTransformer	87.6	86.0	1.6↓

show the robustness and effectiveness of our method on real-world datasets. We hope that our idea of full point encoding will inspire the research community to rethink local and global feature extraction as a single step.

REFERENCES

- Y. Chen, H. Li, R. Gao, and D. Zhao, "Boost 3-d object detection via point clouds segmentation and fused 3-d giou-l1 loss," *IEEE Trans. Neural Netw. Learn. Syst.*, vol. 33, no. 2, pp. 762–773, 2020.
- J. Gao, X. Yan, W. Zhao, Z. Lyu, Y. Liao, and C. Zheng, "Spatio-temporal contextual learning for single object tracking on point clouds," *IEEE Trans. Neural Netw. Learn. Syst.*, 2023.
- D. W. Shu and J. Kwon, "Hierarchical bidirected graph convolutions for large-scale 3-d point cloud place recognition," *IEEE Trans. Neural Netw. Learn. Syst.*, 2023.
- Z. Du, H. Ye, and F. Cao, "A novel local-global graph convolutional method for point cloud semantic segmentation," *IEEE Trans. Neural Netw. Learn. Syst.*, 2022.
- M. U. Khalid, J. M. Hager, W. Kraus, M. F. Huber, and M. Toussaint, "Deep workpiece region segmentation for bin picking," in *Proc. IEEE Int. Conf. Autom. Sci. Eng.* IEEE, 2019, pp. 1138–1144.
- F. J. Lawin, M. Danelljan, P. Tosteberg, G. Bhat, F. S. Khan, and M. Felsberg, "Deep projective 3d semantic segmentation," in *Proc. Int. Conf. Pattern Recognit. Image Anal.* Springer, 2017, pp. 95–107.
- A. Boulch, J. Guerry, B. Le Saux, and N. Audebert, "Snapnet: 3d point cloud semantic labeling with 2d deep segmentation networks," *Comput. Graph.*, vol. 71, pp. 189–198, 2018.
- L. Tchapmi, C. Choy, I. Armeni, J. Gwak, and S. Savarese, "Segcloud: Semantic segmentation of 3d point clouds," in *Proc. Int. Conf. 3D Vis.* IEEE, 2017, pp. 537–547.
- D. Maturana and S. Scherer, "Voxnet: A 3d convolutional neural network for real-time object recognition," in *Proc. IEEE Int. Conf. Intell. Rob. Syst.* IEEE, 2015, pp. 922–928.
- C. R. Qi, H. Su, K. Mo, and L. J. Guibas, "Pointnet: Deep learning on point sets for 3d classification and segmentation," in *Proc. IEEE Conf. Comput. Vis. Pattern Recog.*, 2017, pp. 652–660.
- C. R. Qi, L. Yi, H. Su, and L. J. Guibas, "Pointnet++: Deep hierarchical feature learning on point sets in a metric space," *arXiv preprint arXiv:1706.02413*, 2017.
- Y. Li, R. Bu, M. Sun, W. Wu, X. Di, and B. Chen, "Pointcnn: Convolution on x-transformed points," *Proc. Adv. Neural Inf. Process. Syst.*, vol. 31, pp. 820–830, 2018.
- M. Simonovsky and N. Komodakis, "Dynamic edge-conditioned filters in convolutional neural networks on graphs," in *Proc. IEEE Conf. Comput. Vis. Pattern Recog.*, 2017, pp. 3693–3702.
- S. Wang, S. Suo, W.-C. Ma, A. Pokrovsky, and R. Urtasun, "Deep parametric continuous convolutional neural networks," in *Proc. IEEE Conf. Comput. Vis. Pattern Recog.*, 2018, pp. 2589–2597.
- W. Wu, Z. Qi, and L. Fuxin, "Pointconv: Deep convolutional networks on 3d point clouds," in *Proc. IEEE Conf. Comput. Vis. Pattern Recog.*, 2019, pp. 9621–9630.
- P. Hermosilla, T. Ritschel, P.-P. Vázquez, À. Vinacia, and T. Ropinski, "Monte carlo convolution for learning on non-uniformly sampled point clouds," *ACM Trans. Graph.*, vol. 37, no. 6, pp. 1–12, 2018.
- Y. Shen, C. Feng, Y. Yang, and D. Tian, "Mining point cloud local structures by kernel correlation and graph pooling," in *Proc. IEEE Conf. Comput. Vis. Pattern Recog.*, 2018, pp. 4548–4557.
- H. Thomas, C. R. Qi, J.-E. Deschaud, B. Marcotegui, F. Goulette, and L. J. Guibas, "Kpconv: Flexible and deformable convolution for point clouds," in *Proc. Int. Conf. Comput. Vis.*, 2019, pp. 6411–6420.

- [19] M. Fey, J. E. Lenssen, F. Weichert, and H. Müller, “Splinecnn: Fast geometric deep learning with continuous b-spline kernels,” in *Proc. IEEE Conf. Comput. Vis. Pattern Recog.*, 2018, pp. 869–877.
- [20] Y. Xu, T. Fan, M. Xu, L. Zeng, and Y. Qiao, “Spidernn: Deep learning on point sets with parameterized convolutional filters,” in *Proc. Eur. Conf. Comput. Vis.*, 2018, pp. 87–102.
- [21] H. Lei, N. Akhtar, and A. Mian, “Seggcn: Efficient 3d point cloud segmentation with fuzzy spherical kernel,” in *Proc. IEEE Conf. Comput. Vis. Pattern Recog.*, June 2020.
- [22] S. Xie, S. Liu, Z. Chen, and Z. Tu, “Attentional shapecontextnet for point cloud recognition,” in *Proc. IEEE Conf. Comput. Vis. Pattern Recog.*, 2018, pp. 4606–4615.
- [23] X. Liu, Z. Han, Y.-S. Liu, and M. Zwicker, “Point2sequence: Learning the shape representation of 3d point clouds with an attention-based sequence to sequence network,” in *Proc. AAAI Conf. Artif. Intell.*, vol. 33, no. 01, 2019, pp. 8778–8785.
- [24] J. Yang, Q. Zhang, B. Ni, L. Li, J. Liu, M. Zhou, and Q. Tian, “Modeling point clouds with self-attention and gumbel subset sampling,” in *Proc. IEEE Conf. Comput. Vis. Pattern Recog.*, 2019, pp. 3323–3332.
- [25] J. Lee, Y. Lee, J. Kim, A. Kosiorek, S. Choi, and Y. W. Teh, “Set transformer: A framework for attention-based permutation-invariant neural networks,” in *Proc. Int. Conf. Mach. Learn.* PMLR, 2019, pp. 3744–3753.
- [26] M. Feng, L. Zhang, X. Lin, S. Z. Gilani, and A. Mian, “Point attention network for semantic segmentation of 3d point clouds,” *Pattern Recog.*, vol. 107, p. 107446, 2020.
- [27] X. Yan, C. Zheng, Z. Li, S. Wang, and S. Cui, “Pointasnl: Robust point clouds processing using nonlocal neural networks with adaptive sampling,” in *Proc. IEEE Conf. Comput. Vis. Pattern Recog.*, 2020, pp. 5589–5598.
- [28] H. Zhao, L. Jiang, J. Jia, P. H. Torr, and V. Koltun, “Point transformer,” in *Proc. Int. Conf. Comput. Vis.*, 2021, pp. 16 259–16 268.
- [29] S. Cheng, X. Chen, X. He, Z. Liu, and X. Bai, “Pra-net: Point relation-aware network for 3d point cloud analysis,” *IEEE Trans. Image Process.*, vol. 30, pp. 4436–4448, 2021.
- [30] Q. Hu, B. Yang, L. Xie, S. Rosa, Y. Guo, Z. Wang, N. Trigoni, and A. Markham, “Randla-net: Efficient semantic segmentation of large-scale point clouds,” in *Proc. IEEE Conf. Comput. Vis. Pattern Recog.*, 2020, pp. 11 108–11 117.
- [31] F. Groh, P. Wieschollek, and H. P. Lensch, “Flex-convolution,” in *Proc. Asian Conf. Comput. Vis.* Springer, 2018, pp. 105–122.
- [32] J. Li, B. M. Chen, and G. H. Lee, “So-net: Self-organizing network for point cloud analysis,” in *Proc. IEEE Conf. Comput. Vis. Pattern Recog.*, 2018, pp. 9397–9406.
- [33] F. Engelmann, T. Kontogianni, J. Schult, and B. Leibe, “Know what your neighbors do: 3d semantic segmentation of point clouds,” in *Proc. Eur. Conf. Comput. Vis. Worksh.*, 2018, pp. 0–0.
- [34] F. Engelmann, T. Kontogianni, A. Hermans, and B. Leibe, “Exploring spatial context for 3d semantic segmentation of point clouds,” in *Proc. IEEE Int. Conf. Comput. Vis. Worksh.*, 2017, pp. 716–724.
- [35] Z. Zhang, B.-S. Hua, and S.-K. Yeung, “Shellnet: Efficient point cloud convolutional neural networks using concentric shells statistics,” in *Proc. Int. Conf. Comput. Vis.*, 2019, pp. 1607–1616.
- [36] H. Ran, J. Liu, and C. Wang, “Surface representation for point clouds,” in *Proc. IEEE Conf. Comput. Vis. Pattern Recog.*, 2022.
- [37] X. Ma, C. Qin, H. You, H. Ran, and Y. Fu, “Rethinking network design and local geometry in point cloud: A simple residual mlp framework,” in *Proc. Int. Conf. Learn. Represent.*, 2021.
- [38] H. Zhao, L. Jiang, C.-W. Fu, and J. Jia, “Pointweb: Enhancing local neighborhood features for point cloud processing,” in *Proc. IEEE Conf. Comput. Vis. Pattern Recog.*, 2019, pp. 5565–5573.
- [39] L. Jiang, H. Zhao, S. Liu, X. Shen, C.-W. Fu, and J. Jia, “Hierarchical point-edge interaction network for point cloud semantic segmentation,” in *Proc. Int. Conf. Comput. Vis.*, 2019, pp. 10 433–10 441.
- [40] M. Xu, J. Zhang, Z. Zhou, M. Xu, X. Qi, and Y. Qiao, “Learning geometry-disentangled representation for complementary understanding of 3d object point cloud,” in *Proc. AAAI Conf. Artif. Intell.*, vol. 35, 2021, pp. 3056–3064.
- [41] Y. Wang, Y. Sun, Z. Liu, S. E. Sarma, M. M. Bronstein, and J. M. Solomon, “Dynamic graph cnn for learning on point clouds,” *ACM Trans. Graph.*, vol. 38, no. 5, pp. 1–12, 2019.
- [42] R. Klokov and V. Lempitsky, “Escape from cells: Deep kd-networks for the recognition of 3d point cloud models,” in *Proc. IEEE Int. Conf. Comput. Vis.*, 2017, pp. 863–872.
- [43] M. Xu, Z. Zhou, and Y. Qiao, “Geometry sharing network for 3d point cloud classification and segmentation,” in *Proc. AAAI Conf. Artif. Intell.*, vol. 34, 2020, pp. 12 500–12 507.
- [44] M. Xu, R. Ding, H. Zhao, and X. Qi, “Paconv: Position adaptive convolution with dynamic kernel assembling on point clouds,” in *Proc. IEEE Conf. Comput. Vis. Pattern Recog.*, 2021, pp. 3173–3182.
- [45] Y. Liu, B. Fan, S. Xiang, and C. Pan, “Relation-shape convolutional neural network for point cloud analysis,” in *Proc. IEEE Conf. Comput. Vis. Pattern Recog.*, 2019, pp. 8895–8904.
- [46] C. Wang, B. Samari, and K. Siddiqi, “Local spectral graph convolution for point set feature learning,” in *Proc. Eur. Conf. Comput. Vis.*, 2018, pp. 52–66.
- [47] X. Wu, Y. Lao, L. Jiang, X. Liu, and H. Zhao, “Point transformer v2: Grouped vector attention and partition-based pooling,” *arXiv preprint arXiv:2210.05666*, 2022.
- [48] Y. Ma, Y. Guo, H. Liu, Y. Lei, and G. Wen, “Global context reasoning for semantic segmentation of 3d point clouds,” in *Proc. IEEE Winter Conf. Appl. Comput. Vis.*, 2020, pp. 2931–2940.
- [49] H. Lei, N. Akhtar, and A. Mian, “Spherical kernel for efficient graph convolution on 3d point clouds,” *IEEE Trans. Pattern Anal. Mach. Intell.*, 2020.
- [50] S. Qiu, S. Anwar, and N. Barnes, “Semantic segmentation for real point cloud scenes via bilateral augmentation and adaptive fusion,” in *Proc. IEEE Conf. Comput. Vis. Pattern Recog.*, 2021, pp. 1757–1767.
- [51] L. Tang, Y. Zhan, Z. Chen, B. Yu, and D. Tao, “Contrastive boundary learning for point cloud segmentation,” in *Proc. IEEE Conf. Comput. Vis. Pattern Recog.*, 2022, pp. 8489–8499.
- [52] X. Lai, J. Liu, L. Jiang, L. Wang, H. Zhao, S. Liu, X. Qi, and J. Jia, “Stratified transformer for 3d point cloud segmentation,” in *Proc. IEEE Conf. Comput. Vis. Pattern Recog.*, 2022, pp. 8500–8509.
- [53] J. Choe, C. Park, F. Rameau, J. Park, and I. S. Kweon, “Pointmixer: Mlp-mixer for point cloud understanding,” in *Proc. Eur. Conf. Comput. Vis.* Springer, 2022, pp. 620–640.
- [54] G. Qian, Y. Li, H. Peng, J. Mai, H. Hammoud, M. Elhoseiny, and B. Ghanem, “Pointnext: Revisiting pointnet++ with improved training and scaling strategies,” in *Proc. Adv. Neural Inf. Process. Syst.*, 2022.
- [55] S. Fan, Q. Dong, F. Zhu, Y. Lv, P. Ye, and F.-Y. Wang, “Scf-net: Learning spatial contextual features for large-scale point cloud segmentation,” in *Proc. IEEE Conf. Comput. Vis. Pattern Recog.*, 2021, pp. 14 504–14 513.
- [56] I. Armeni, O. Sener, A. R. Zamir, H. Jiang, I. Brilakis, M. Fischer, and S. Savarese, “3d semantic parsing of large-scale indoor spaces,” in *Proc. IEEE Conf. Comput. Vis. Pattern Recog.*, 2016, pp. 1534–1543.
- [57] A. Dai, A. X. Chang, M. Savva, M. Halber, T. Funkhouser, and M. Nießner, “ScanNet: Richly-annotated 3d reconstructions of indoor scenes,” in *Proc. IEEE Conf. Comput. Vis. Pattern Recog.*, 2017, pp. 5828–5839.
- [58] B. Graham, M. Engelcke, and L. Van Der Maaten, “3d semantic segmentation with submanifold sparse convolutional networks,” in *Proc. IEEE Conf. Comput. Vis. Pattern Recog.*, 2018, pp. 9224–9232.
- [59] M. Jaritz, J. Gu, and H. Su, “Multi-view pointnet for 3d scene understanding,” in *Proc. Int. Conf. Comput. Vis. Worksh.*, 2019, pp. 0–0.
- [60] H.-Y. Chiang, Y.-L. Lin, Y.-C. Liu, and W. H. Hsu, “A unified point-based framework for 3d segmentation,” in *Proc. Int. Conf. 3D Vis.*, 2019, pp. 155–163.
- [61] W. Hu, H. Zhao, L. Jiang, J. Jia, and T.-T. Wong, “Bidirectional projection network for cross dimension scene understanding,” in *Proc. IEEE Conf. Comput. Vis. Pattern Recog.*, 2021, pp. 14 373–14 382.
- [62] C. Choy, J. Gwak, and S. Savarese, “4d spatio-temporal convnets: Minkowski convolutional neural networks,” in *Proc. IEEE Conf. Comput. Vis. Pattern Recog.*, 2019, pp. 3075–3084.
- [63] C. Park, Y. Jeong, M. Cho, and J. Park, “Fast point transformer,” in *Proc. IEEE Conf. Comput. Vis. Pattern Recog.*, 2022, pp. 16 949–16 958.
- [64] A. Geiger, P. Lenz, C. Stiller, and R. Urtasun, “Vision meets robotics: The kitti dataset,” *Int J Rob Res.*, vol. 32, no. 11, pp. 1231–1237, 2013.
- [65] M. Contributors, “Mmdetection3d: Openmmlab next-generation platform for general 3d object detection,” <https://github.com/open-mmlab/mmdetection3d>, 2020.
- [66] Z. Zhang, B. Sun, H. Yang, and Q. Huang, “H3dnet: 3d object detection using hybrid geometric primitives,” in *Proc. Eur. Conf. Comput. Vis.* Springer, 2020, pp. 311–329.
- [67] I. Misra, R. Girdhar, and A. Joulin, “An end-to-end transformer model for 3d object detection,” in *Proc. Int. Conf. Comput. Vis.*, 2021, pp. 2906–2917.
- [68] B. Cheng, L. Sheng, S. Shi, M. Yang, and D. Xu, “Back-tracing representative points for voting-based 3d object detection in point clouds,” in *Proc. IEEE Conf. Comput. Vis. Pattern Recog.*, 2021, pp. 8963–8972.

- [69] Y. Wang, X. Chen, L. Cao, W. Huang, F. Sun, and Y. Wang, "Multimodal token fusion for vision transformers," in *Proc. IEEE Conf. Comput. Vis. Pattern Recognit.*, 2022, pp. 12 186–12 195.
- [70] H. Wang, S. Shi, Z. Yang, R. Fang, Q. Qian, H. Li, B. Schiele, and L. Wang, "Rbgnet: Ray-based grouping for 3d object detection," in *Proc. IEEE Conf. Comput. Vis. Pattern Recognit.*, 2022, pp. 1110–1119.
- [71] C. R. Qi, O. Litany, K. He, and L. J. Guibas, "Deep hough voting for 3d object detection in point clouds," in *Proc. Int. Conf. Comput. Vis.*, 2019, pp. 9277–9286.
- [72] Z. Liu, Z. Zhang, Y. Cao, H. Hu, and X. Tong, "Group-free 3d object detection via transformers," in *Proc. Int. Conf. Comput. Vis.*, 2021, pp. 2949–2958.
- [73] S. Shi, X. Wang, and H. Li, "Pointcnn: 3d object proposal generation and detection from point cloud," in *Proc. IEEE Conf. Comput. Vis. Pattern Recognit.*, 2019, pp. 770–779.
- [74] S. Shi, C. Guo, L. Jiang, Z. Wang, J. Shi, X. Wang, and H. Li, "Pv-rnn: Point-voxel feature set abstraction for 3d object detection," in *Proc. IEEE Conf. Comput. Vis. Pattern Recognit.*, 2020, pp. 10 529–10 538.
- [75] Z. Wu, S. Song, A. Khosla, F. Yu, L. Zhang, X. Tang, and J. Xiao, "3d shapenets: A deep representation for volumetric shapes," in *Proc. IEEE Conf. Comput. Vis. Pattern Recog.*, 2015, pp. 1912–1920.
- [76] M. A. Uy, Q.-H. Pham, B.-S. Hua, T. Nguyen, and S.-K. Yeung, "Revisiting point cloud classification: A new benchmark dataset and classification model on real-world data," in *Proc. Int. Conf. Comput. Vis.*, 2019, pp. 1588–1597.
- [77] Y. Ben-Shabat, M. Lindenbaum, and A. Fischer, "3dmfv: Three-dimensional point cloud classification in real-time using convolutional neural networks," *IEEE Robot. Autom. Lett.*, vol. 3, no. 4, pp. 3145–3152, 2018.
- [78] S. Qiu, S. Anwar, and N. Barnes, "Dense-resolution network for point cloud classification and segmentation," in *Proc. IEEE Winter Conf. Applications of Computer Vision*, 2021, pp. 3813–3822.
- [79] Qiu, Shi and Anwar, Saeed and Barnes, Nick, "Geometric back-projection network for point cloud classification," *IEEE Trans. Multimedia*, 2021.
- [80] M. Atzmon, H. Maron, and Y. Lipman, "Point convolutional neural networks by extension operators," *ACM Trans. Graph.*, vol. 37, no. 4, pp. 1–12, 2018.
- [81] Z. Liu, H. Hu, Y. Cao, Z. Zhang, and X. Tong, "A closer look at local aggregation operators in point cloud analysis," in *Proc. Eur. Conf. Comput. Vis.* Springer, 2020, pp. 326–342.
- [82] L. Fan, Z. Pang, T. Zhang, Y.-X. Wang, H. Zhao, F. Wang, N. Wang, and Z. Zhang, "Embracing single stride 3d object detector with sparse transformer," in *Proc. IEEE Conf. Comput. Vis. Pattern Recognit.*, 2022, pp. 8458–8468.